Solvatochromism and turn-off fluorescence sensing property of N, N'- Bis (3-Pentyl) Perylene-3, 4, 9, 10-bis(dicarboximide) towards Nitroaromatics and photophysical study of its microstructures

4.1. Introduction

Perylene-based pigments have been found applications as high quality varnish with superb light fastness [186, 187] due to their luminous colors and their long-term chemical stability. All the members of poly aromatic hydrocarbon (PAHs) and perylenediimides (PDIs) derivatives have been studied more extensively [188] because of their extended rigid planar backbones, π-conjugation, extreme luminescence, photochemical and surprising thermal stability which reveal exclusive self-assembly behaviors and high charge-carrier mobility [189]. In addition to their strong light-harvesting and fluorescence properties, PDIs have found increasing applications in chemical sensing [190], organic light-emitting diodes (OLEDs) [191], organic field-effect transistors (OFETs) [192, 193] etc. Many organic luminophores are highly emissive in dilute solution, but their emission decreases with increasing concentration in solution or in aggregated state due to strong intermolecular π-π stacking interaction and collision induced non-radiative decay [194-196]. This phenomenon is known as the aggregation caused quenching (ACQ) effect.

Much effort has been dedicated to synthesize organic nano/microparticles of various sizes and shapes. These include zero dimensional (0-D) spherical or tetrahedral quantum dots [197-202], one-dimensional (1-D) nano rods and wires from small organic compounds [203-205], two-dimensional (2-D) nanoplates [206], micro rods, bars, plates, panicle [207, 208], nanoribbons and nanotube [209], submicrotubes [210], organic nanoflowers [211] and three dimensional highly symmetrical small molecular organic microcrystals with shapes ranging from cubes through truncated cubes to rhombic dodecahedra [212] etc. Various methods were developed to prepare organic nano/microparticles, such as reprecipitation [213-2015], solid phase reaction [216], Molecular beam deposition[217], electro-spinning[218], template method [219], laser ablation [220], self-organization [221], physical vapor deposition [222] etc. Among the above-mentioned methods, reprecipitation is one of the favoured routes towards the cost-effective large-scale production of nano/micro building blocks.

Selective sensors for detection of nitro-aromatic compounds (NACs) in particular 2,4,6-trinitrotoluene (TNT), 2,4-dinitrotoluene (DNT) and 2,4,6-trinitrophenol (picric acid, PA) are

of enormous curiosity in both environmental protection and national security because they are not only due to many unexploded land mines worldwide but also predictable as toxic to living organisms [223]. In current years, enormous hard work have been devoted to expand new fluorescent materials or π conjugated molecule with a variety of sensing mechanisms for detecting explosives in order to realize super-sensitivity, as well as fast response time [224]. Physical detection methods for explosives include gas chromatography coupled with a mass spectrometer [225], energy-dispersive X-ray diffraction, surface enhanced Raman spectroscopy [226], nuclear quadruple resonance [227] and electron capture detection [228]. These techniques are highly selective, but moderately complex and involve expensive instrumentation. Mainly detection methods for explosives are only pertinent to vapor samples because of interfering problems encountered in complex aqueous media.

In this present communication, we report Solvatochromic effect of N, N'-Bis (3-Pentyl) Perylene-3, 4, 9, 10-bis (dicarboximide) [**P^2**] in different polar solvent with high fluorescence emission intensity. The intense emission behavior of **P^2** is being used for the selective sensing of picric acid among the nitro-aromatics. Photo physical properties of the aqueous dispersion of **P^2** microstructures are investigated using UV–Vis absorption and steady state as well as time resolved fluorescence emission measurements. The fluorescence spectra of **P^2** aggregated hydrosol exhibits Both E-type and Y-type excimer emission band. **P^2** microstructures also exhibits optical wave guides property under ultraviolet irradiation. The absorption and fluorescence spectra of **P^2** in good solvents changes with the polarity of the solvent. This dyes exhibits different color when it is diluted. But the novelty of this work is that **P^2** exhibits Solvatochromism effect, optical wave guides property and also selective sensor activity towards picric acid in neat solvent at a concentration as low as 3.0 μM. The drastic decrease in fluorescence intensity of **P^2** in the presence of PA has been explained due to ground state complexation between **P^2** and PA.

4.2. Experimental Section

4.2.1. Materials

N, N'-Bis (3-Pentyl) Perylene-3, 4, 9, 10-bis (dicarboximide) [**P^2**] was purchased from Sigma-Aldrich Chemical Corp. Sodium dodecyl sulphate (SDS) was purchased from Merck India Ltd and was recrystallized from 1:1 ethanol water mixture. Tetrahydrofuran (THF) was obtained from S. D. Fine-Chem Ltd and was distilled from sodium /benzophenone under argon atmosphere to make it free from moisture, oxygen and peroxide. Picric acid (PA), dinitro benzene (DNB), 4-nitrophenol (NP), 2, 4-dinitrophenol (DNP), 3, 5-

dinitrobenzoic acid (3, 5-DNBA) and 2, 4-dinitro toluene (DNT) were purchased from E-Merck India Ltd. The purity of these chemicals was checked spectrophotometrically. Triply distilled deionized water was used throughout the experiment.

4.2.2. Synthesis of P^2 Microparticles

The microstructures of **P^2** were synthesized by re-precipitation method and SDS is used as morphology directing agent. In a typical synthesis, small volume of 15μM **P^2** in THF was injected into 5 mL of continuously stirred water and aqueous SDS separately at room temperature (25°C) for 5 min. Clearness of the solution was gradually decreased with increasing concentration of **P^2** and a milky reddish color was appeared. The solution was allowed to stand for overnight. Concentration of both **P^2** and SDS were varied to synthesize **P^2** microstructures. During the synthesis of sample-a, b, c, d, e, f, g, & h concentration of SDS (3.96 mM) were kept constant and that of **P^2** (sample-a: 0.14μM, sample-b: 0.29μM, sample-c: 0.84μM, sample-d: 1.36μM, sample-e: 2.5μM, sample-f: 2.9μM, sample-g: 3.4μM, sample-h: 3.8μM) was varied in order to study the effect of **P^2** concentration on aggregated structures. Similar synthesis of **P^2** microstructures was done in the absence of SDS and the samples are named as sample-a1 to h1 respectively. On the other hand, sample-i & j were prepared by injecting 1.75 mL of 15μM **P^2** in THF into 5 mL 10mM SDS and 5 mL 20mM SDS with constant stirring respectively.

4.2.3. Characterization

UV-Vis spectroscopic measurements were carried out in a 1cm quartz cuvette with a Shimadzu UV-1800 spectrophotometer. Fluorescence spectra were recorded using Hitachi F-7000 Fluorescence Spectrophotometer. The Morphologies of the synthesized nano/microstructures were studied using a ZEISS EVO 18 Scanning Electron Microscope (SEM) with an accelerating voltage of 5 kV. Samples for the SEM study were prepared by placing a drop of the aqueous suspension of particles on a small glass slide followed by solvent evaporation under vacuum. To minimize sample charging, the dried samples were coated with a thin gold layer right before SEM study. Time-resolved fluorescence measurements were carried out under ambient conditions using a time-correlated single-photon counting (TCSPC) spectrometer [a picosecond diode laser (IBH, UK)] with the detection wavelength at 529 nm for **P^2** both in presence and absence of picric acid (Ex wavelength 376 nm). We also carried out life time measurements of **P^2** in cyclohexane (522 nm), THF (530 nm), DMF (537 nm) and aggregated hydrosol of **P^2** in water at 615 nm, 675 nm. Excitation wavelength was 455 nm for all the samples. Lamp profiles were measured

with a band-pass of 3 nm using Ludox as scatterer. The decay parameters were recovered using non-linear iterative fitting procedure based on the Marquardt algorithm [229].The quality of fit was assessed over the entire decay, including the rising edge, and tested with a plot of weighted residuals and other statistical parameters e.g. the reduced $\chi 2$ ratio [230]. The signal was detected at magic angle (54.7°) polarization using a Hamamatsu MCP PMT (3809U). Time resolution of the experimental setup was ~90 ps. Optical microscopy images were taken using an NIKON ECLIPSE LV100POL upright microscope equipped with CCD camera (model no. Nikon DS-Fi l), polarizer-analyzer assembly and 100W mercury lamp as excitation source for emission study. The samples for optical microscopic study were prepared by placing a drop of the as prepared hydrosol onto a clean glass slide. XRD was recorded in a 'Rigaku Miniflex-II' X-ray diffractometer using CuKα radiation (λ=0.154056nm). Scans were collected on dry samples in the range of 30-200. Samples for the XRD study of aggregated hydrosol were prepared by drying aqueous suspension of particles on a small glass slide followed by solvent evaporation under vacuum.

4.2.4. Computational method

Ground state geometry of $\mathbf{P^2}$ was optimized by Density Functional Theory (DFT) based hybrid functional (B3LYP) with 6-31G(d) basis set. All the computations in this present study were carried out using Gaussian-09 software package program [231].

4.2.5. Detection Limit

The detection limit was calculated on the basis of the fluorescence titration. The fluorescence emission spectrum of $\mathbf{P^2}$ as a function of its increasing concentration was measured five times, and the standard deviation (σ) of the blank measurement was calculated. To obtain the slope (k), the fluorescence emission intensity at 530 nm was plotted against the increasing concentration of quencher i.e, picric acid in the present study. The detection limit was calculated using the following equation [232],

$$\text{Detection limit} = 3\sigma/k$$

4.3. Results and Discussion

4.3.1. Solvatochromic Study

Fig. 4.1a and ***4.1b*** shows the UV-Vis absorption and fluorescence emission spectra of $\mathbf{P^2}$ in different solvents with increasing polarity. Both the spectra show bathochromic shift with the increasing polarity of the solvent. The mirror image relationship between absorption and emission spectra in each solvent indicate that apart from solvent polarity effect, no other

photochemical processes take place in the excited state of **P²**. Time resolve fluorescence emission study of **P²** shows (***see Fig. 4.2***) that the emission lifetime changes from 385 ps to 415 ps to 421 ps as we change the solvent polarity from cyclohexane to THF to DMF.

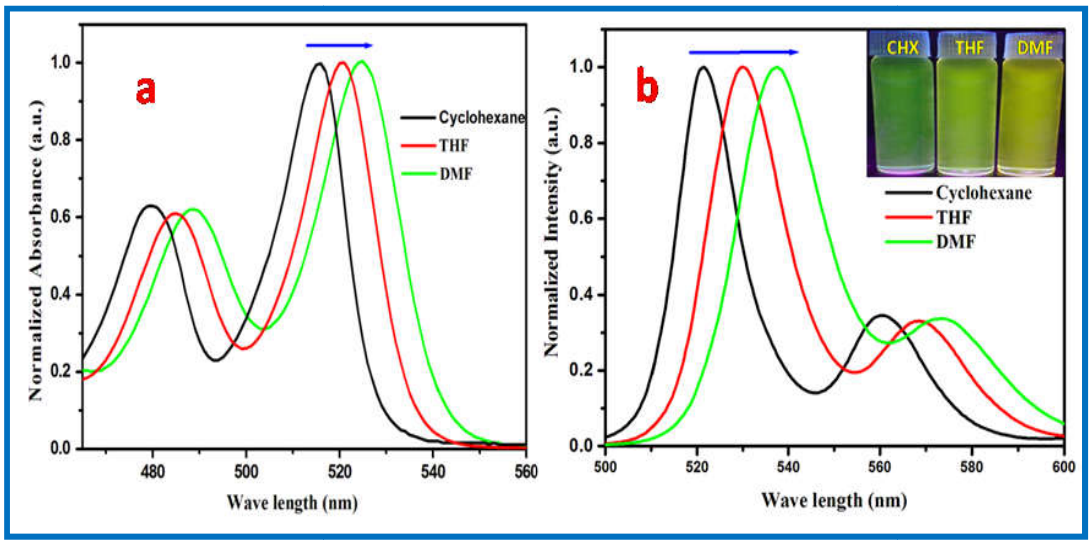

Fig. 4.1: (a) UV-visible absorption spectra and (b)Fluorescence Spectra of **P²** in different solvent; cyclohexane (black line), THF (red line), DMF (green line). Inset: picture taken during UV light illumination to **P²** solutions in various solvents. λ_{ex} = 365 nm.

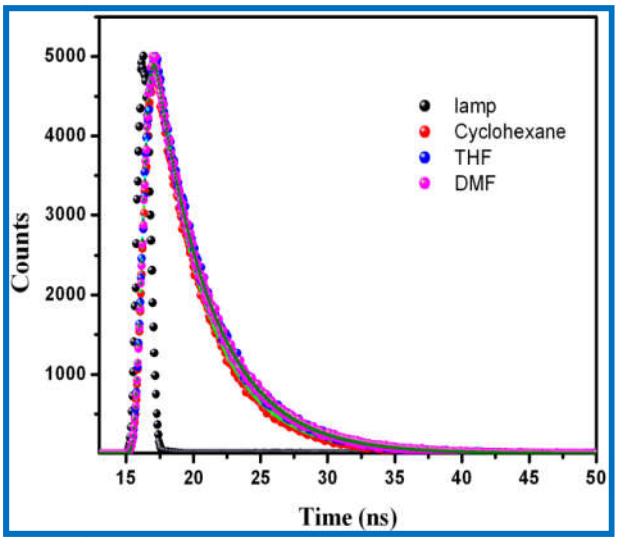

Fig. 4.2: Fluorescence life time of **P²** in different solvent. Excitation: 455 nm, Emission: 522 nm (cyclohexane),530 nm (THF),537 nm(DMF).

Keeping this in mind, we did solvatochromic study of **P²** to get an idea of its excited state polarity. We have used the following form of Lippert Mataga [233, 234] equation.

$$\bar{\nu}_A - \bar{\nu}_f \approx \frac{2}{hc_0}\left(\frac{\varepsilon-1}{2\varepsilon+1} - \frac{n^2-1}{2n^2+1}\right) \times \left(\frac{(\mu_e-\mu_g)^2}{a^3}\right) + \text{Constant} \qquad \text{.....(1)}$$

All the symbols in the above equation have their usual significances. Our computed Onsager cavity radius as the average diameter of the optimized structure of **P²** using DFT/B3LYP- 6-31G level of theory is found to be 7.5 Å. The Stokes shifts (Δν, = ν_A- ν_f) of the absorption and emission peak maximum and the orientation polarizability (Δ*f*), for different solvent polarity are listed in table-2.

$$\Delta f = [(\varepsilon - 1)/(2\varepsilon + 1) - (n^2 - 1)/(2n^2 + 1)]$$

The plot of stokes shift (Δν) vs. orientation polarizability (Δ*f*) is linear as shown in (***Fig. 4.3c***). Solvatochromism (***Fig. 4.3a*** & ***4.3b***) correspond to bathochromic shift with increasing solvent polarity and it depends on the difference in dipole moment of the molecule between its excited & ground state. The observed change of dipole moment from Lippert-Mataga plot is found to be 1.27 D. This signifies that **P²** is a polar molecule with moderate change of dipole moment upon electronic excitation.

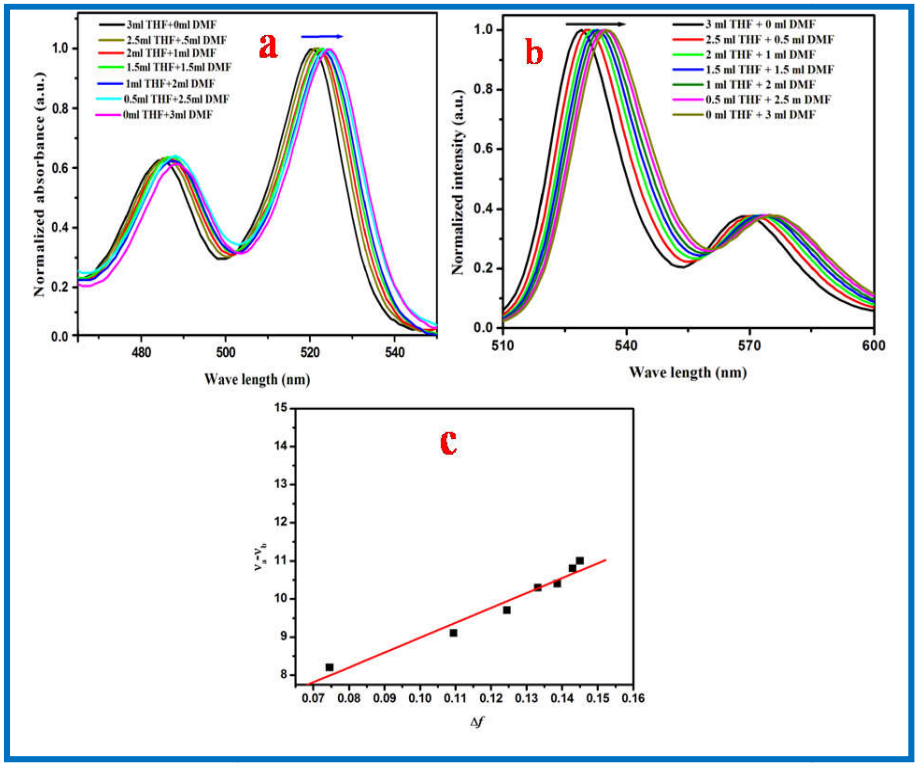

Fig. 4.3: (a) UV-Vis absorption spectra of **P²** in various proportion of THF-DMF mixture. (b) Fluorescence emission spectra of **P²** in various proportion of THF-DMF mixture. (c) Plot of the Stokes shift of **P²** vs. the orientation polarizability (Δ*f*) of solvent (THF-DMF) mixtures.

4.3.2. Concentration Dependence Photophysical Study of P²

Fluorescence emission spectra with increasing concentration of **P²** in THF are shown in ***Fig. 4.4a.*** A large red shift of emission spectra are observed as the concentration changes from 1.5×10^{-5} M to 8×10^{-3} M. Structured emission having vibronic peaks at 529, 575 and 615

nm are observed when the concentration of **P²** is as low as 1.5×10^{-5} M. Intensity of the structured vibronic band decreases and a broad band with peak at 626 nm is appeared with the increasing concentration of **P²** from 1.5×10^{-5} M to 8×10^{-4} M to 10×10^{-4} M. Further increases of concentration to 8×10^{-3} M results a broad emission band with peak at ~ 640 nm. This type of red shifted broad emission band with increasing concentration of fluorophore is known as excimer emission. There are some reports in the literature that **P²** can form two types of excimer, i.e. Y excimer and E excimer [235] depending upon the orientations of two approaching molecules.

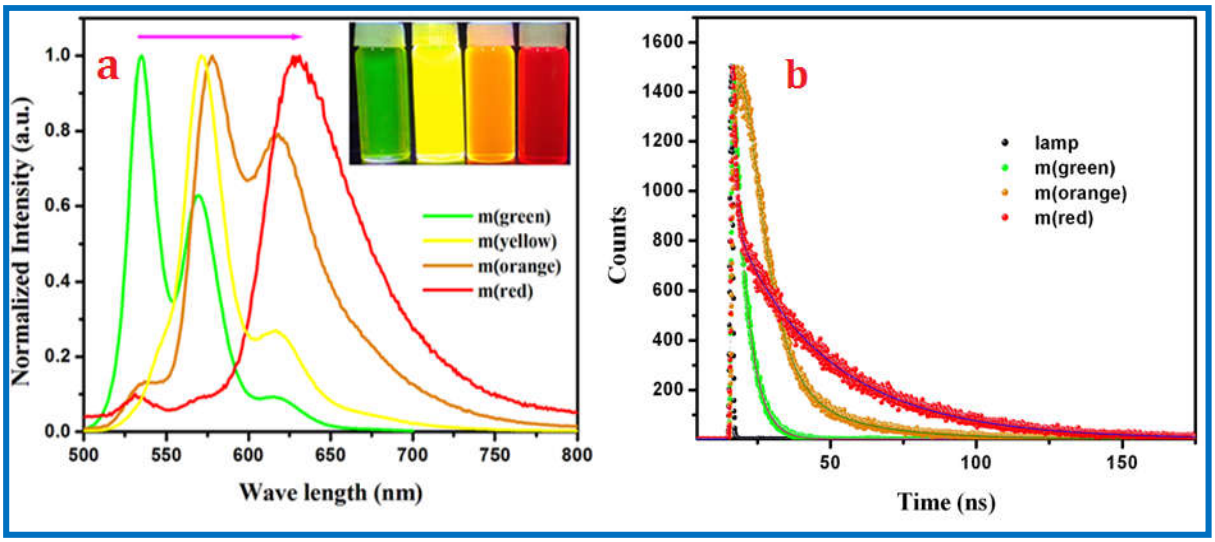

Fig. 4.4: (a) Concentration dependent luminescence of **P²** in THF. The concentrations from left to right are: 1.5×10-5, 8×10-4, 1.0×10-3 and 8×10-3 M. Inset: Pictures taken during illumination of UV light (365 nm) to different concentration of **P²** (b) Fluorescence life time of **P²** having different concentration in THF. Excitation: 455 nm, Emission: 530,578,630 nm.

Since the extent of π- stacking interaction of the face to face E- excimer is more, the red shifted broad band is due to E-type excimer. On the other hand the oblique orientations of two **P²** molecules cause less stacking, and hence comparatively the less red shifted emission band due to Y-type excimer is observed. Our fluorescence lifetime measurement study (***Fig. 4.4b***) of the samples having different concentration of **P²** show that at very low concentration, the monomeric fluorescence emission (λ_{em} = 529 nm) having lifetime 4.5 ns is observed (Table-1). Now as the fluorescence is monitored at the peak position (575 nm) for a slightly higher concentration of **P²**, a biexponential fit is required to analyze the fluorescence decay curve. The major component having 6 ns fluorescence lifetime is due to monomeric decay from the singlet excited state of **P²** and the 25 ns component is due to Y excimer emission of **P²** are observed. On the other hand, a 34 ns major component along with a faster one (2 ns) are observed at 640 nm and this 34 ns component arises from the E-excimer of **P²**.

4.3.3. Sensing of nitroaromatics:

UV-Vis absorption studies of **P²** upon gradual addition of PA show the appearance of new band at 550 nm with the increasing level-off tail in the visible region. (***Fig. 4.5***) It is observed that the emission intensity at ~ 550 nm increases and that of at 520 nm gradually decreases with the increasing concentration of picric acid to the solution. Our study also revealed that there is no significant change in UV-Vis absorption spectra to all nitroaromatic compounds because their electron deficiency cannot reach to such extent to form ground state complex with **P²**.

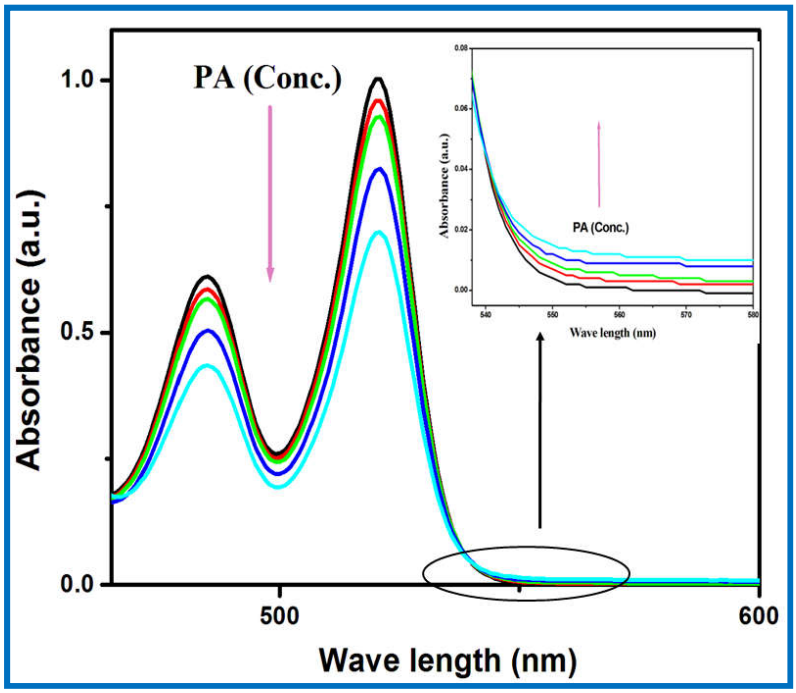

Fig. 4.5: UV-Vis absorbance spectra of **P²** (3.0×10^{-5}M in THF) in presence of PA in THF.

The fluorescence emission spectrum of **P²** in THF exhibits structured emission band with peak at 530, 570 and 615 nm. Fluorescence intensity of **P²** decreases with the increasing concentration of picric acid (***Fig. 4.6a***). Among the variety of nitro derivatives studied [2,4-dinitrotolune (DNT), 2,4-dinitrophenol (DNP), dinitrobenzene (DNB), 3,5-dinitrobenzoic acid (DNB), 4-nitrophenol (NP)]; the maximum quenching of **P²** emission is observed in case of picric acid (PA). It is observed that the PL intensity of **P²** decreases with the increasing concentration of PA in the solution but the PL spectra position remain unchanged (***Fig. 4.6a***).

The fluorescence quenching results can also be evaluated with the Stern-Volmer equation, $I_0/I=1+K_{sv}[Q]$, where K_{sv} is the Stern-Volmer quenching constant. A linear Stern−Volmer plot was obtained when concentration of PA is below 30×10^{-5}M (inset of fig.4 b). But, at a higher concentration of PA, the plot bent upward (***Fig. 4.6b***), indicating

superamplified quenching effect [236]. The Stern-Volmer quenching constant (K_{sv}) of PA (6.02×10^3 M^{-1}) is almost similar to the other reported chemosensors for picric acid [237]. We have measured fluorescence lifetime of **P^2** in the absence and presence of PA as shown in ***Fig. 4.6c***. All excitation are done at 337 nm and emissions are measured at 529 nm.

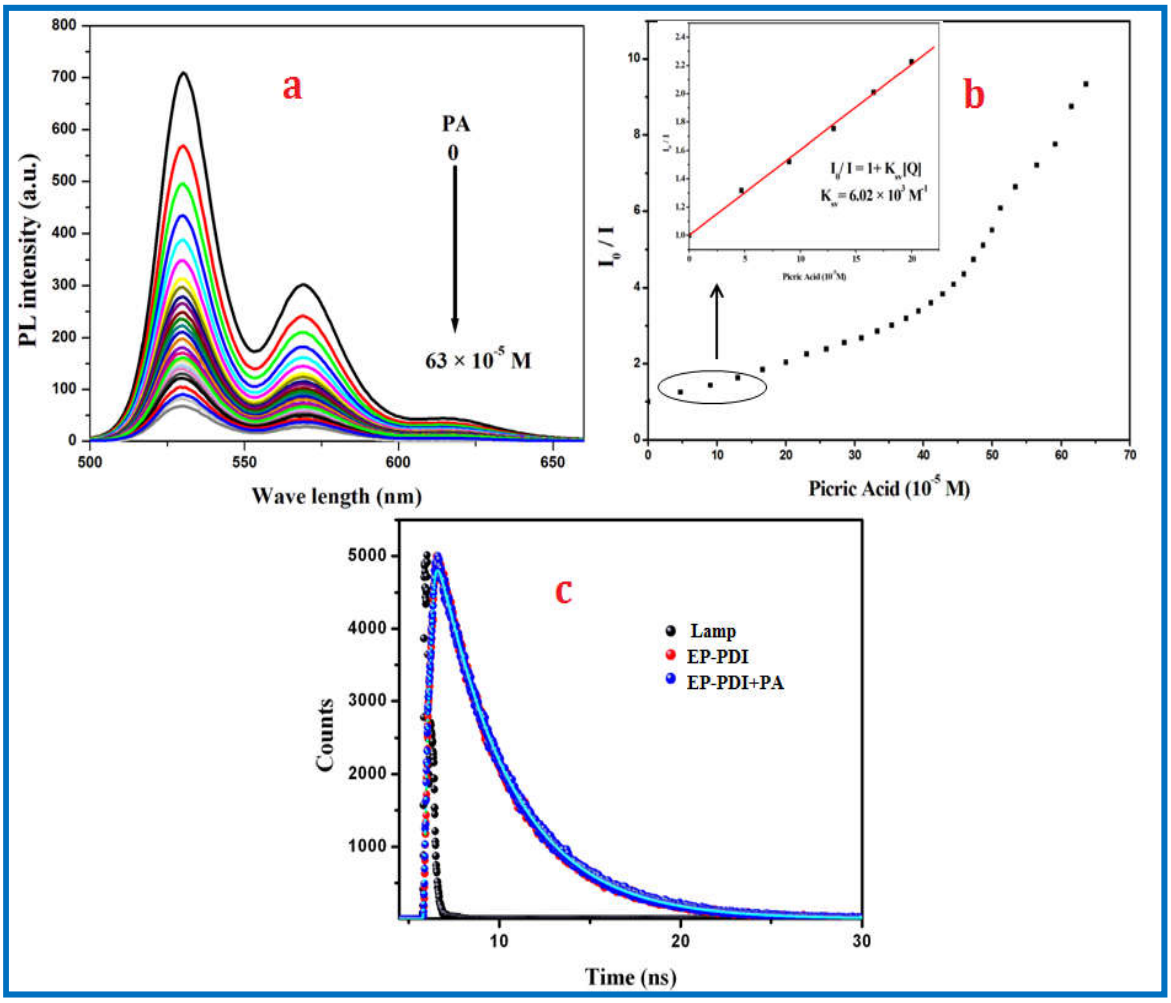

Fig. 4.6: (a) Fluorescence emission spectra of **P^2** (1.36μM in THF) in presence of increasing concentration (0-300 μM) of picric acid (PA), λex = 455 nm. (b) Plot of I0/ I Vs. [PA] for **P^2** in THF (Insert show Stern-Volmer curve of corresponding fluorescence quenching in presence of different amount of PA) (c) Fluorescence decay profiles of **P^2** in THF and **P^2** in presence 62 μM PA; λem = 529nm. All emission spectra were taken with 337 nm excitation.

The fluorescence decay curve of **P^2** in THF is fitted with single exponential decay and the observed decay time is 3.93 ns. On the other hand fluorescence lifetime of **P^2** (at 529 nm) in presence of PA shows single components having measured lifetime 4.00 ns. Thus fluorescence lifetime values remain unchanged and the fitted components are identical for both the cases. It indicates that the quenching is static in nature and ground state complex is formed between **P^2** and PA. For static quenching, $\tau_0/\tau = 1$; in contrast, fluorescence intensity $F_0/F = \tau_0/\tau$ for dynamic quenching [224].

Fluorescence quenching studies of **P²** with various nitro aromatics show that for a fixed concentration (35.4 × 10^{-5}M) of nitroaromatics, PA only drastically quenches the fluorescence intensity of **P²**. Inset of ***Fig. 4.7a*** shows the PL images of the solution of **P²** contacting different nitroaromatics upon UV-illumination. Almost no emission is observed from the solution containing PA. This suggested that PA is the strong quencher of **P²** emission and this turn off fluorescence emission of **P²** by PA can be used as selective sensor to detect trace amount of PA present in solution. Among the nitroaromatics used in this present study, PA is strong electron acceptor and hence it shows strong affinity to form ground state complex with **P²**. Our measured quenching efficiency (%) (***Fig. 4.7b***) by different nitroaromatics show that PA (70%) is the strongest and then followed by DNP(22%), DNB(12%), DNBA(10%), DNT (8%) and NP(7%).We further measured the limit of detection of PA using 3σ method and the detection limit is found to be 2.98 μM.

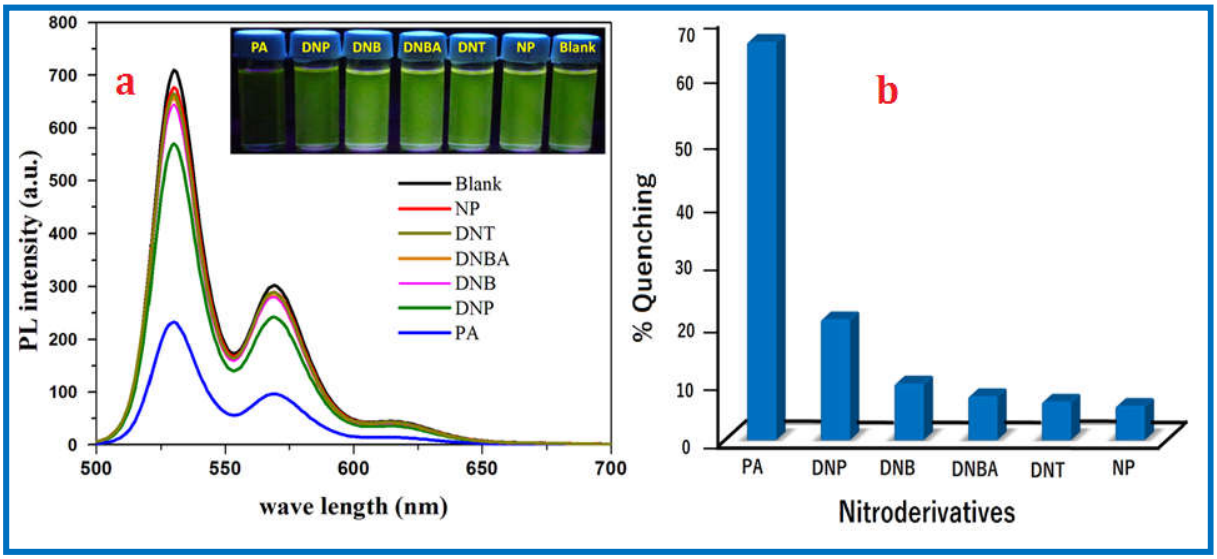

Fig. 4.7: (a) Fluorescence emission spectra of **P²** (1.36μM in THF) upon addition of different nitro-derivatives (35.4 × 10-5M). Inset: UV light illumination of **P²** in presence of different nitro-derivatives. λex = 365 nm. (b) Percentage quenching of fluorescence intensity of **P²** (1.36μM in THF) after the addition of fixed concentration (35.4 × 10-5M) of various nitro-derivatives.

4.3.4. SEM study of aggregated hydrosol

We did two set of synthesis where the concentration of SDS and **P²** were varied for a fixed concentration of **P²** and SDS respectively. Our SEM study (***Fig. 4.8***) reveals that the morphology of particles is rod shaped at lower **P²** concentration and the shape of the perylene microstructure changes from rod to fibroid with increasing **P²** concentration. We have also synthesized **P²** micro structured in the absence of SDS using similar experimental conditions

(see ***Fig. 4.9***). In the absence of SDS, fibroid like microstructures with less thickness are obtained compare to presence of SDS.

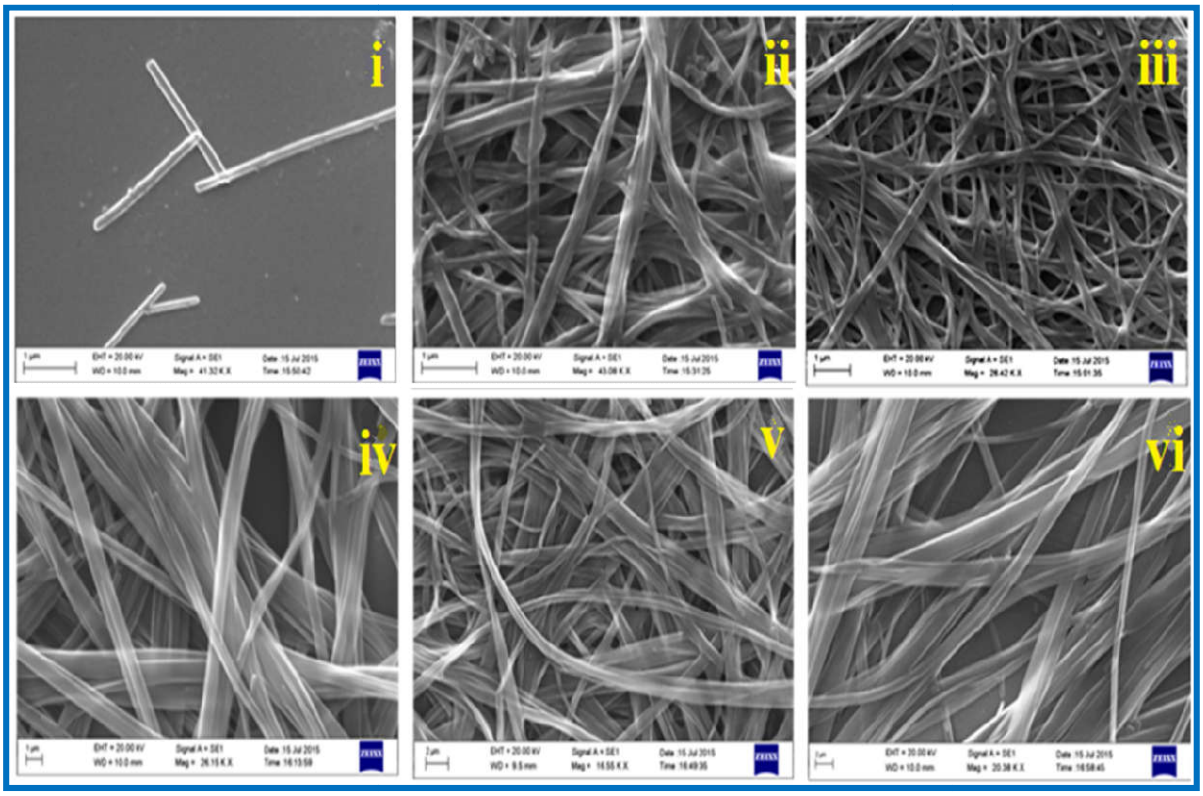

Fig. 4.8: SEM images of $\mathbf{P^2}$ microstructures with SDS (i) sample-d, (ii) sample-e, (iii) sample-g, (iv) sample-h, (v) sample-i, (vi) sample-j.

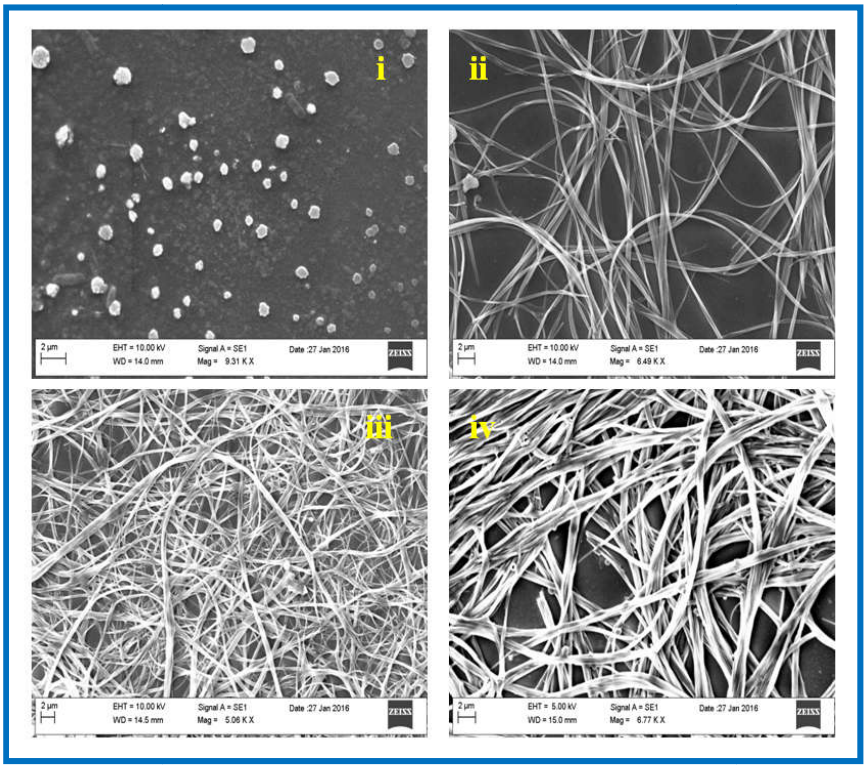

Fig. 4.9: SEM images of $\mathbf{P^2}$ microstructures without SDS (i) sample-d1, (ii) sample-e1, (iii) sample-g1, (iv) sample-h1,

4.3.5. Optical microscopic study of aggregated hydrosol

Intense solid-state luminescence of **P^2** microcrystals is observed during fluorescence optical microscopic study. Fiber shaped morphologies are clearly observed from the sample-e, g, h, i, j using optical microscopy (***Fig. 4.10***). At low **P^2** concentration, particle sizes are too small to be detected by the present resolution of our optical microscope. Upon UV excitation, micro crystals having clear edges with reddish luminescence are observed. The morphology of **P^2** microstructure in all the samples are fiber like and there is a clear indication that dimension of the particles increases in two directions (length & width) with the increasing concentration of **P^2**. We also obtained similar optical images of **P^2** microstructures in the absence of SDS, but the clarity of optical images at lower **P^2** concentration is not as good as it is in presence of SDS (see ***Fig. 4.11***).

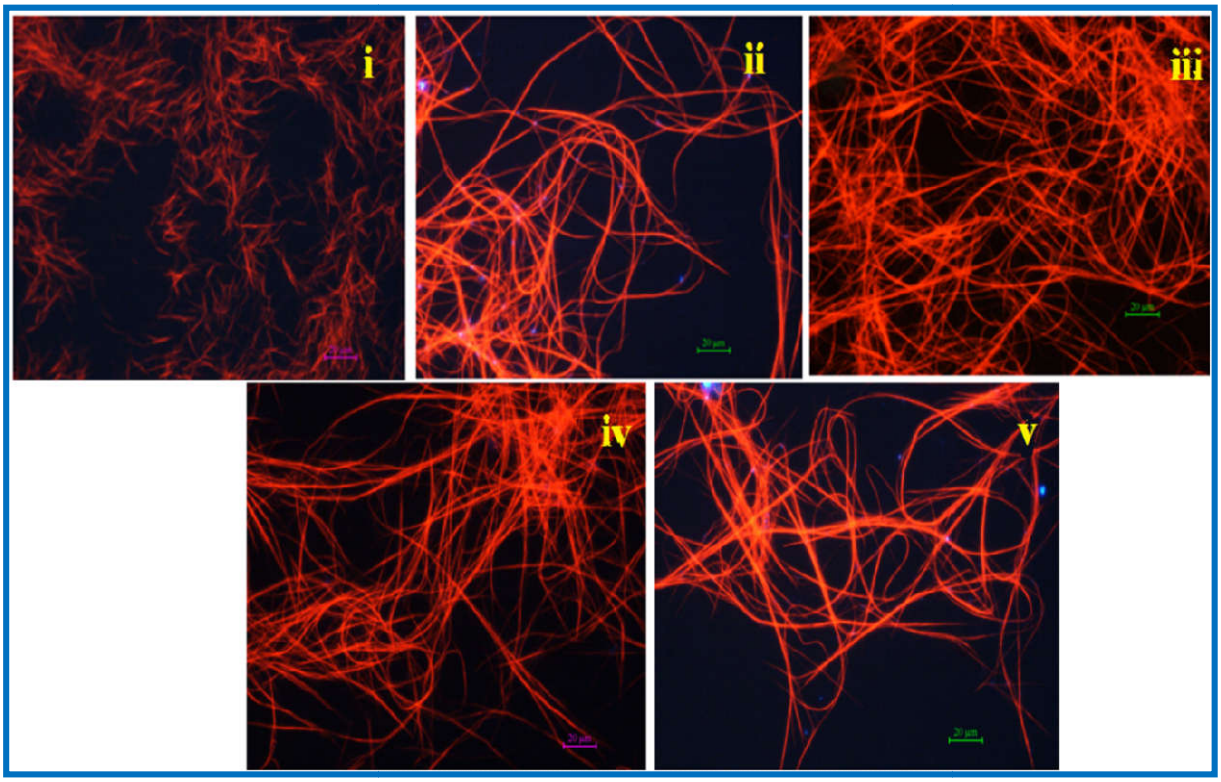

Fig. 4.10: Optical fluorescence microscopy images under UV illumination of **P^2** microstructures with SDS (i) sample-e, (ii) sample-g (iii) sample-h (iv) sample-i and (v) sample-j.

4.3.6. XRD Study of aggregated hydrosol

XRD study was carried out in order to re-check the crystalline nature of sample -h_1 (***Fig. 4.12***). We have tried our best to grow single crystal of **P^2** in the present experimental condition, but we failed. On the other hand we have compared our powder XRD data of **P^2** with the one obtained from the single crystal data as reported by M. Wiatrowski et al [238]. XRD peaks at different 2θ values as shown in fig. 8 are in agreements with the XRD spectra

reported by Wiatrowski et al [238]. Thus it is confirmed that our synthesized microcrystals have monoclinic unit cell geometry.

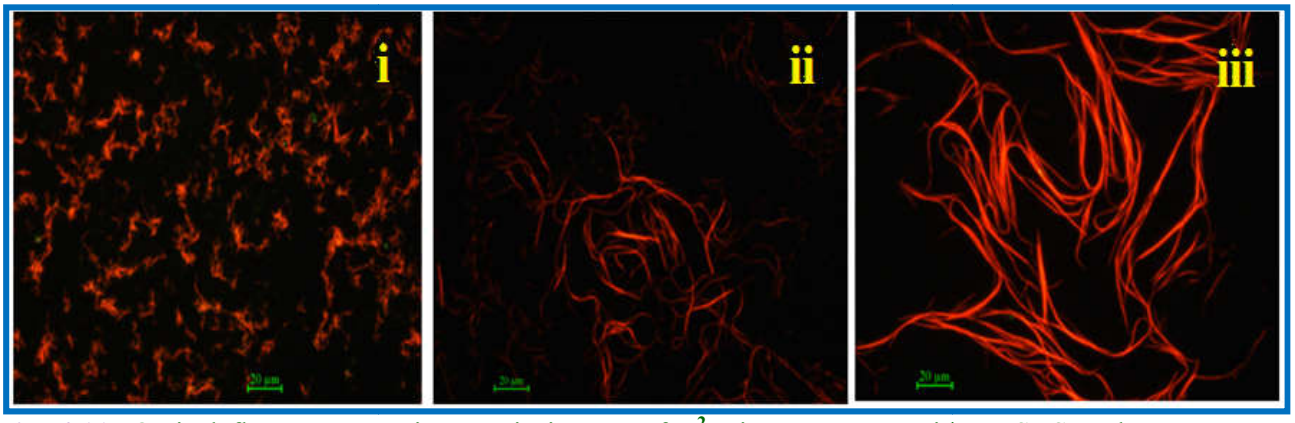

Fig. 4.11: Optical fluorescence microscopic images of $\mathbf{P^2}$ microstructures without SDS under UV illumination (i) sample-e_1, (ii) sample-g_1 and (iii) sample-h_1.

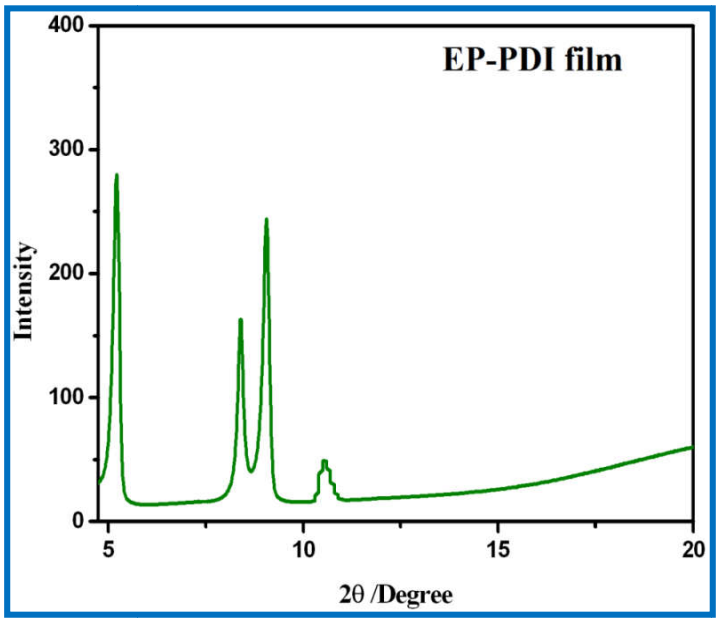

Fig. 4.12: XRD patterns of film prepared from the microcrystal of sample-h_1.

4.3.7. UV-Vis Study of aggregated hydrosol

In case of Polyaromatic hydrocarbon like anthracene, pyrene etc, the group of bands with higher energy are associated primarily with excitation direction along the long (a, a') axis and the group of band with lower energy are associated with excitation direction along the short (b, b') axis (***Scheme 4.1***) [239]. The UV absorption spectrum of $\mathbf{P^2}$ can be divided into two well distinct regions, located at 410-550 nm and 255-370 nm and this spectrum corresponds to two types of electronic transitions (***Fig. 4.13***) [240]. The spectrum stems from molecular transition at 410-540 nm directed along the long axis of the perylene chromophore. Vibrational peaks starting at 368 nm to the peak at 260 nm correspond to transition along the

short axis of perylene chromophore. Three distinct vibronic transition at 520 (0,0), 485 (0,1) and 454 (0,2) are observed in the absorption spectra of $\mathbf{P^2}$ (***Fig. 4.13***). The absorption spectrum of $\mathbf{P^2}$ hydrosols shows overall broadening in the region 410-600 nm. The broadening and red shift of the spectra indicate strong π-π interaction among the neighbouring $\mathbf{P^2}$ molecules. In addition, the overall shift of the spectral baseline of samples a-h relative to that of the monomer is attributed to the scattering of light by the larger aggregated structures in solution (***Fig. 4.13***).

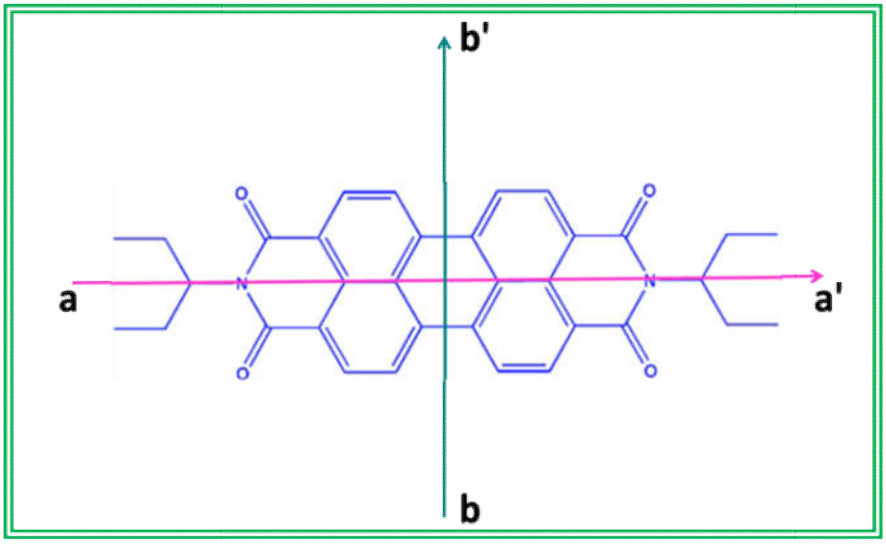

Scheme 4.1. $\mathbf{P^2}$ with its long (a, a') and short (b, b') axis.

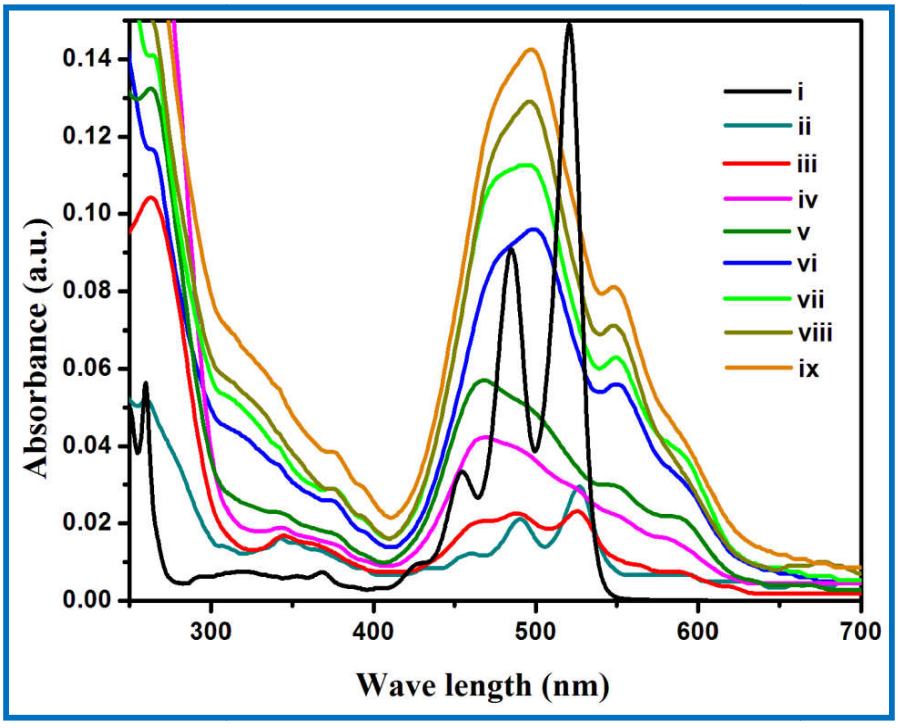

Fig. 4.13: The UV-visible absorption spectra of (i) $\mathbf{P^2}$ in THF (ii) sample-a, (iii) sample-b, (iv) sample-c, (v) sample-d, (vi) sample-e, (vii) sample-f, , (viii) sample-g, , (ix) sample-h.

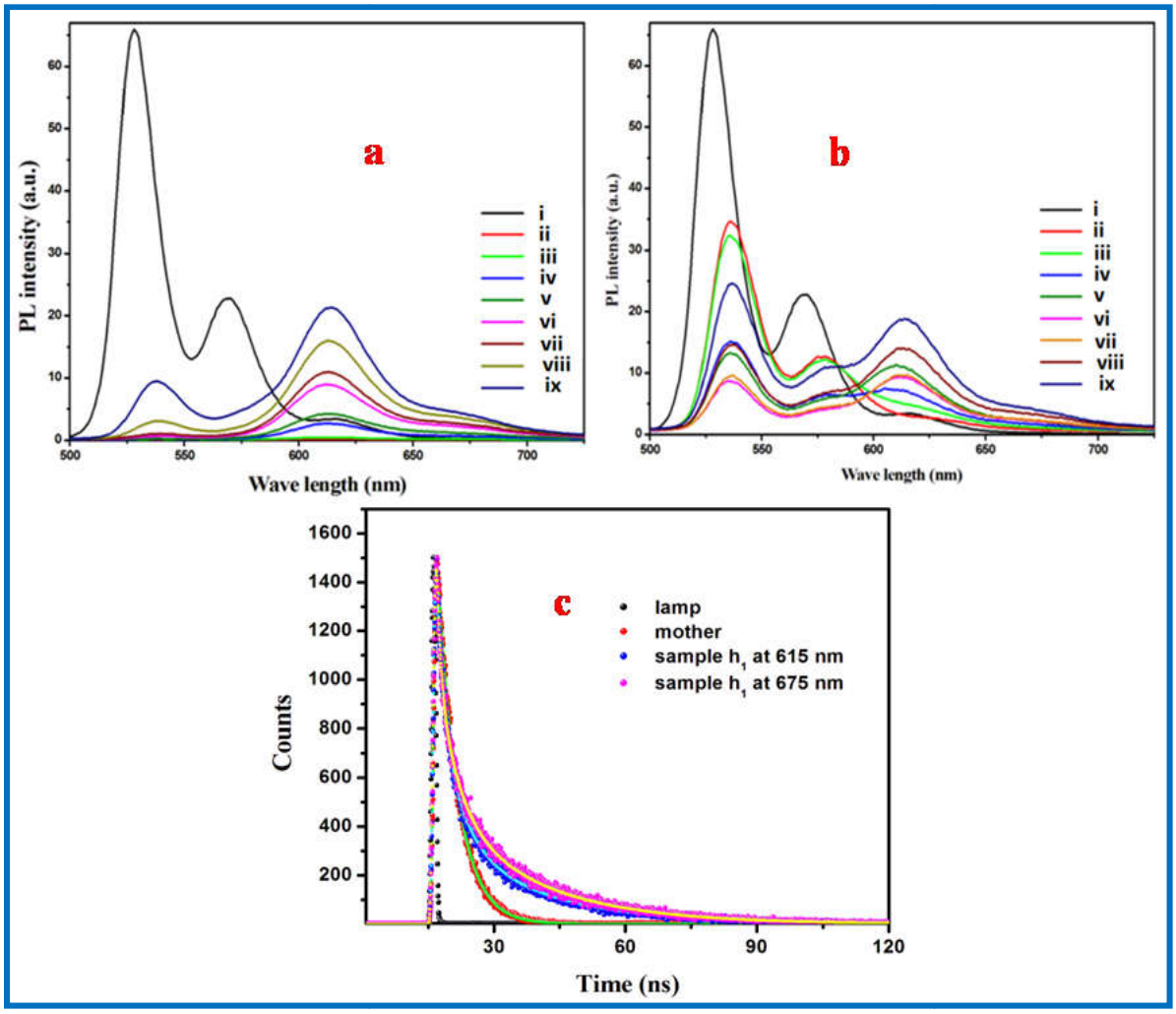

Fig. 4.14: (a) Fluorescence emission spectra of (i) $\mathbf{P^2}$ in THF, (ii) sample-a_1 (iii) sample-b_1 (iv) sample-c_1 (v) sample-d_1 (vi) sample-e_1. (vii) sample-f_1, (viii) sample-g_1, (ix) sample-h_1. λex = 455 nm. (b) Fluorescence emission spectra of (i) $\mathbf{P^2}$ in THF, (ii) sample-a (iii) sample-b (iv) sample-c (v) sample-d (vi) sample-e. (vii) sample-f, (viii) sample-g, (ix) sample-h. λex = 455 nm (c) Fluorescence life time of $\mathbf{P^2}$ in THF and its aggregated hydrosols (sample-h1); λex = 455 nm, λem= 615, 675 nm.

4.3.8. Emission Study of aggregated hydrosol

PL spectra of $\mathbf{P^2}$ in THF and the aggregated hydrosol of $\mathbf{P^2}$ are shown in (***Fig. 4.14a***). It is observed that the dilute solution (1.36μM) of $\mathbf{P^2}$ in THF exhibits structured emission band with peaks at 530, 570 and 615 nm upon 455 nm photo excitation. The distinct mirror image relationship between the UV-Vis absorption and fluorescence emission spectra of $\mathbf{P^2}$ suggests that $\mathbf{P^2}$ is structurally rigid with little displacement of molecular geometry in its electronically excited state. Fluorescence emission spectra of the aggregate hydrosol ***Fig. 4.14a*** shows that the structure emission band decreases and sharp red shifted emission band due to Y and E type excimer is appeared at 615 nm and 675 nm respectively. Time resolved fluorescence study (***Fig. 4.14c***) from both 615 and 675 nm emission show that there are two emission components. A faster component having 3-4 ns lifetime for both cases (615 nm &

675 nm emission) arises due to **P^2** present in free State in the solution. The longer one i.e the 19 ns component at 615 nm emission is due to Y type excimer and the 21.4 ns component at 675 nm is due to E type excimer emission. On the other hand emission from the hydrosol in the presence of SDS (***Fig. 4.14b***), show a quenching of the structured emission band and two broad band one at 615 nm and the other at 675 nm are appeared due to Y and E type of excimer respectively.

4.4. Conclusion

In this work, we report the Solvatochromic effect in the PL spectra of **P^2** molecule in THF-DMF mixture. **P^2** in THF shows structured fluorescence emission and aggregated hydrosol exhibits both E-type and Y-type excimer emission. The intense emission property of **P^2** is used as sensor for detecting nitroaromatics particularly PA present at a very low concentration in the solution. The detection limit of **P^2** for PA has been determined using 3σ method and our obtained detection limit is 2.98 μM. On the other hand aggregated hydrosol of **P^2** exhibits strong excimer emission at longer wave length ~ 615 nm due to molecular association. The intense red shifted emission from the aggregated hydrosol of **P^2** has been explained due to Y and E- type excimer emission. This type emission is further substantiated using time resolved fluorescence study.